Construction and Building Materials 281 (2021) 122550

Contents lists available at ScienceDirect

Construction and Building Materials

journal homepage: www.elsevier.com/locate/conbuildmat

# Potential anti-vibration pavements with damping layer: Finite element (FE) modeling, validation, and parametrical studies

Jiandong Huang [a,b], Massimo Losa [b], Pietro Leandri [b], Shiva G. Kumar [b], Junfei Zhang [c], Yuantian Sun [a,*]

[a] School of Mines, China University of Mining and Technology, 221116 Xuzhou, China
[b] Department of Civil and Industrial Engineering, University of Pisa, 56125 Pisa, Italy
[c] School of Civil and Transportation Engineering, Hebei University of Technology, 300401 Tianjin, China

## HIGHLIGHTS

- Potential anti-vibration pavements with damping layer.
- Vibration evaluation based on FE analysis.
- Novel characterization method for damping property.
- Parametrical analysis for anti-vibration pavements.

## ARTICLE INFO

*Article history:*
Received 3 November 2020
Received in revised form 27 January 2021
Accepted 28 January 2021
Available online 23 February 2021

*Keywords:*
Dynamic analysis
Rayleigh damping
Pavement
Response
Shear beam model

## ABSTRACT

Vibrations induced by traffic are of concern for road authorities due to disturbance on the population, and the damage of buildings and structures. In the field of pavement engineering, the anti-vibration paving technologies by the so-called *damping layer* are under investigation to avoid the generation of excessive vibration and contains propagation. To more fully examine the effectiveness and potential of such a damping layer in the application of anti-vibration pavement, numerical simulations based on a two-dimensional (2D) finite element (FE) model is conducted. The method of determining Rayleigh damping parameters is proposed to more accurately characterize the attenuation of vibration in the road pavements. Sensitivity analysis of varying monitored points and varying loads are performed. Several important parameters such as the damping layer position and thickness, damping ratio are evaluated as well. By the use of this FE simulation to model the vibration response induced by traffic, the costly construction mistakes and field experimentation can be avoided.



## 1. Introduction

The convenient transportation has enriched people's lives. However, vibration-induced by road traffic is around everyone in the city, which can affect the living conditions of urban residents and can lead to sleep disorders, and is becoming more and more serious. Traffic-induced vibration can jeopardize the integrity and the stability of historical buildings [1–4]. Vibrations are to be reduced also in the case of sensitive scenarios as hospitals, scientific research labs, and high-tech industries [5–9]. Furthermore, road vibrations can induce traffic-generated noise dominating frequencies below 1000 Hz [10,11]. Therefore, reducing vibrations is of primary interest.

To mitigate the effects of traffic-induced vibration, various preventive strategies are under investigation. Limiting traffic volumes and speed, screening of vibration by using in-ground barriers, and developing isolation systems, represent some of the methods proposed [6]. In the field of pavement engineering, the so-called anti-vibration paving technology is under investigation to avoid the generation of excessive vibration [12]. To preserve an ancient building (the Villa Farnesina, Roma) against traffic-induced vibrations, an anti-vibration system composed of a concrete grid supported by rubber pads, was developed under the near Lungotevere road, reducing the acceleration values of about 80% according to the obtained results. Similar solutions have also been used for new constructions in Piazzetta S. Paolo, Milan, and Via Parigi, Roma [2]. The anti-vibration pavement has also been developed by Dondi et al. [13] and Grandi [14] with a lower-stiffness vibration-absorbing layer which did not reduce the stiffness of the whole pavement systems. Such anti-vibration pavement has

* Corresponding author.
*E-mail addresses:* huang@cumt.edu.cn (J. Huang), losa@ing.unipi.it (M. Losa), junfeizhang2010@gmail.com (J. Zhang), yuantiansun@cumt.edu.cn (Y. Sun).

https://doi.org/10.1016/j.conbuildmat.2021.122550
0950-0618/

been proved to increase the elastic absorption capacity of the vibrations caused by the surface irregularities near the source. Based on the optimized surface texture as well as the improvement of the vibration absorbing, another type of anti-vibration pavement was constructed for the Municipality of Novara [12]. The verification was conducted by the vibration comparison of the anti-vibration pavement and one reference, showing the anti-vibration level reached. Diependaele and Rens proposed an ambitious design for a tramway carriageway consisting of continuously reinforced concrete having a three-layered structure supported on a noise and vibration abatement mat [15]. The results showed that the propagation of acoustic waves and vibration waves through the sub-soil to nearby houses, schools, and commercial buildings was prevented by providing a flexible insulating mat underneath and against the sides of the concrete railway slab.

In 2019, a novel trial pavement for anti-vibration was designed and constructed by Huang and co-workers. The test track was located in Via Dino Buzzati, Agliana (Prato, Italy). The trial field covered 24 m in length and 6 m in width in which the existing wearing course has been fully milled. The field construction was divided into two parts, each of which included test sections of 8 m (with damping layer) and 16 m (without damping layer), respectively. The damping layer is composed of so-called damping asphalt mixtures (DAMs) with a thickness of 3 cm. A detailed introduction to the DAMs can be found in early studies [9,16–19]. The on-site falling weight deflectometer (FWD) test was used to simulate the vibration response of the traffic pulse load to the surrounding environment [20–22]. The results show that laying a damping layer composed of DAMs in the road system can effectively reduce the vibration response of the loads to the surrounding environment, indicating the applicability of such kind of damping layer in anti-vibration pavements.

The trial field experiment on anti-vibration pavement showed the effectiveness in mitigating the vibration response of the surrounding environment caused by traffic loads [16]. However, the process of field experiments is often expensive and time-consuming. Therefore, it is difficult to be carried out many times to investigate the design parameters to achieve reasonable optimization of the anti-vibration pavements. Furthermore, the effectiveness of vibration-reduction was only evaluated from the deflection in the time domain and the effectiveness and potential of the damping layer cannot be fully evaluated [20–22].

To more fully examine the potential and effectiveness of the damping layer in the application of anti-vibration and optimize the pavement structure, the study presented in this paper involves the creation and analysis of a two-dimensional (2D) finite element (FE) modeling of road pavements based on the field tests to dynamically analyze the vibration reduction.

The research plan of the present study is given in Fig. 1. (I) the dynamic analysis of flexible pavement is the starting point of the simulation. However, it should be noted that the conventional method used for the dynamic analysis may need to be improved since it rarely involves the accurate vibration-calculation in road pavements while often focuses on the stress–strain states at different locations. Besides, as indicated by Chopra [23], the conventional method for damping characterization is not appropriate if the system to be analyzed consists of two or more parts with significantly different levels of damping, such as the pavement include a special damping layer. Therefore, the damping characterization is a prerequisite for the vibration calculation in the road pavements [24,25]. Based on such consideration, (II) a novel method for determining the Rayleigh damping parameters is proposed to improve the deficiencies in previous studies. The accuracy of the method is verified by the comparison with the results of field testing. (III) Once the damping characterization is completed, a 2D-based FE dynamic model of pavement subjected to the pulse load can be established. A traditional pavement and an anti-vibration one are compared to emphasize the effect of the damping layer, and at the same time, parametrical studies are carried out to evaluate the effects of the varying thickness, location, and damping ratio of materials used.

## 2. Damping characterization in flexible pavement

### 2.1. Literature review

#### 2.1.1. Damping characterization in finite element (FE) modeling

The dynamic analysis has been successfully used to predict the pavement response more accurately under different traffic load conditions while considering a wide range of constitutive laws based on the finite element (FE) modeling, during which the procedures for creating stiffness and mass matrices for a system's elements and their assembly into a global system representation have been well established [26]. However, analogous procedures for representing intrinsic damping, a material's innate capability for mechanical energy dissipation, are still under development [24,27–32]. A material's intrinsic damping does not refer to a unique phenomenon but rather to a collection of atomic actions that produce an observable effect on a system's overall dynamic response [33–38]. It is not currently practical for typical engineering purposes to link these actions at the atomic level to the overall system response. Therefore, intrinsic damping is typically modeled on the material scale, considering constitutive and rheological properties.

A very common and efficient type of damping used in the incremental finite element modeling for pavement engineering is Rayleigh damping, giving damping matrix [C] as the combination of mass-proportional damping and stiffness proportional damping, as shown in Equation (1) [39,40].

$$[C] = \alpha[M] + \beta[K] \tag{1}$$

where $[M]$, $[C]$, and $[K]$ are the mass matrix, damping matrix, and stiffness matrix, respectively; $\alpha$ and $\beta$ are mass proportional parameter and stiffness proportional parameter, respectively. The relationship between $\alpha$ and $\beta$ and the critical-damping ratio at a

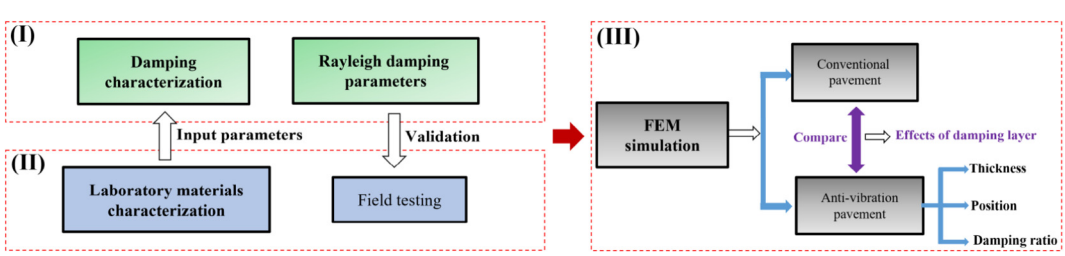


**Fig. 1.** Research plan in the present study.

circular frequency ω for one degree of freedom problem is given by Equation (2) [41,42].

$$\xi = \frac{\alpha}{2\omega} + \frac{\beta\omega}{2} \tag{2}$$

where $\xi$ is the damping ratio and $\omega$ is the circular frequency [rad/s]. Damping is an important component of the material's behavior; it must be considered in dynamic problems that include loading with FWD or moving wheels while it can be ignored in static problems [43]. For the dynamic analysis, so far several researchers have tried to get meaningful values of Rayleigh damping coefficients α and β, and the methods can be divided into two situations:

(1) In the first type of method, the damping matrix for each layer is assembled, where the frequency range considered is that of the whole system. Typically, in this method, the natural frequency of the road system is determined firstly, then the classical damping matrix to represent each layer or each material is calculated by Rayleigh damping and the global damping matrix is assembled via standard FE techniques [39,44–47]. The study conducted by Uddin and Garza [40] showed the natural frequency to range from 3.7 Hz for a thin highway pavement to 14.7 Hz for a thick airport pavement. In the same study, the Rayleigh damping parameters are determined as $\alpha = 4.86\ s^{-1}$ and $\beta = 4.85 \times 10^{-5}$ s by the assumption of a damping ratio of 5% and the natural frequency of 8 Hz. Ling and Newcomb [44] set α = 0 and calculated β for a single degree of freedom problem using a damping ratio of 5% and a natural frequency of 14 Hz as suggested by Mamlouk [48] and Davies and Mamlouk [20]. Siddharthan et al. [22] used α = 0 and β = 0.002 for a damping ratio of 6% to 9% and a natural frequency of 10 to 15 Hz. The weakness of this type of method has been pointed out by Wang et al. [30] that it can result in a non-orthogonal global damping matrix, thus obscuring the meaning of the mode shape and natural frequency between the sub-components and the entire system and ignoring the interaction of sub-components.

(2) In the second type of method, the natural frequency of each layer is calculated firstly by the assumption of a free-free boundary condition. Wang and Yang [49] set $\alpha = 0.078\ s^{-1}$ and β = 0.0321 s by the calculation of the natural frequency of 1.56 Hz for the AC layer and $\alpha = 0.086\ s^{-1}$ and β = 0.0291 s by the calculation of the natural frequency of 1.72 Hz for subgrade. Zeng [47] set β = 0 and calculated α as 25, 8, 0.125 $s^{-1}$ for rubber-modified asphalt concrete (RMAC), asphalt concrete (AC) and compacted soil, respectively. This type of method suffers from the drawback that it is frequencies of the two lacking an effective method to calculate the natural frequency of each subcomponent, which may result in large errors compared to actual conditions. Besides, the method to separate each sub-component also ignores the interactions between sub-components. Besides, the results obtained from Valaskova et al. showed large dispersion of the Rayleigh coefficients, especially of alpha at the lower bulk densities, but the overall trend leads to smaller dispersion at higher densities [50].

In summary, the damping characterization in the dynamic analysis is not well established, and it is difficult to determine the natural frequencies and modal damping ratios that might be more applicable to the general flexible pavement. Since there is no uniform, effective, and reasonable method to calculate Rayleigh parameters, it can lead to large differences in the determined values which may cause different dynamic responses. In any case, once the above-mentioned natural frequency and modal damping are selected, the next process is to determine the corresponding Rayleigh damping parameters.

#### 2.1.2. Determination of the Rayleigh damping parameters

Typically, there are two principal methods for determining Rayleigh damping parameters to be used in FEM analyses. The first one was proposed and applied by Idriss [51] in the QUAD4 software for geotechnical seismic analysis then applied in pavement dynamics [49,52]. It was assumed that the contributions of mass and stiffness proportional coefficients are the same. In this way, α and β can be described as,

$$\alpha = \xi_1 \omega_1 \tag{3}$$

$$\beta = \frac{\xi_1}{\omega_1} \tag{4}$$

where $\xi_1$ is the damping ratio and $\omega_1$ is the fundamental frequency of the system. The relationship between frequency and damping ratio is given in Fig. 2, from which it can be observed that such a method can results in an overestimation of damping in all frequency ranges, determining a lower dynamic response of the system.

Hudson et al. [53] introduced appropriate improvements to these shortcomings of using only the fundamental frequency to determining the damping coefficient and modified the QUAD4 as QUAD4M, which has been applied in some research of pavement dynamics as well [39,46]. Two natural frequencies $\omega_1$ and $\omega_2$ are determined for the calculation of the Rayleigh damping parameters. Particularly, $\omega_1$ is the first fundamental frequency, and $\omega_2 = n\omega_1$, where $n$ is an odd number greater than $\omega_e/\omega_1$; $\omega_e$ is the dominant frequency. The parameters α and β are given as follows.

$$\alpha = 2\xi \frac{\omega_1 \omega_2}{\omega_1 + \omega_2} \tag{5}$$

$$\beta = 2\xi \frac{1}{\omega_1 + \omega_2} \tag{6}$$

As shown in Fig. 3, this method takes the natural frequencies and spectral characteristics of the structure into considerations, but can underestimate the damping between $\omega_1$ and $\omega_2$ as well as overestimate damping outside that range.

### 2.2. Proposed model for damping characterization in flexible pavement

The following section describes the development of the proposed model for damping characterization in the flexible pavement, consisting of two main steps, (1) According to the method proposed by Liang et al. [54], to characterize the damping difference between different layers, the multi-layered pavement structure is divided into sub-layers, each of which consists of materials of similar physical properties. Then each sub-layer is treated as a subsystem for damping characterization, by selecting the corresponding Rayleigh damping parameters. (2) Rayleigh damping parameters are determined to make sure the target damping ratio (the small-strain material damping) and modal damping calculated from natural frequencies match best by linear

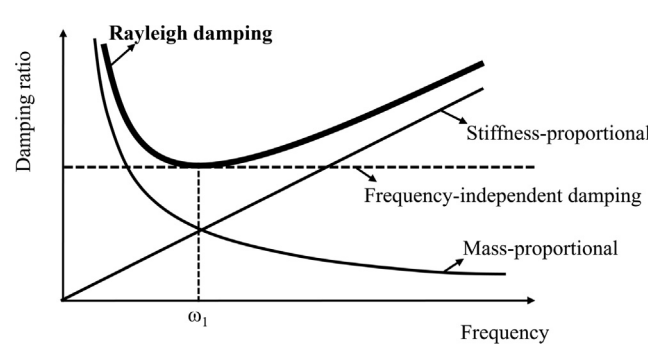


**Fig. 2.** Relationship between damping and frequency by QUAD4.

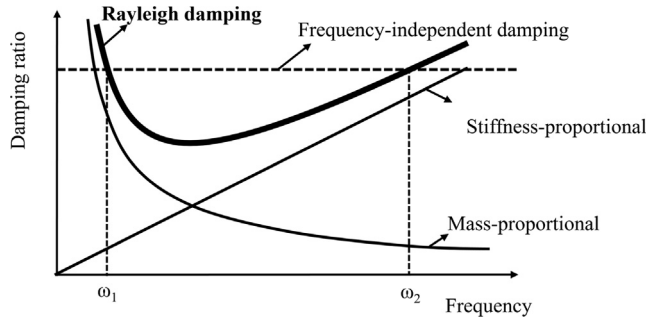


**Fig. 3.** Relationship between damping and frequency by QUAD4M.

time-domain solutions [55]. A detailed description of the proposed method is described below.

*2.2.1. Division of road structure and calculation of natural frequencies for each part*

As a multilayer system, the road structure consists of finite layers over a semi-infinite subgrade. The layered site of the different pavement materials properties has significantly different damping. To characterize the difference between different layers, the road pavement can be divided into several sub-layers depending on the materials, and each sub-layer is chosen with the corresponding Rayleigh damping parameters [54]. For a typical pavement structure, according to similar physical properties of the materials, the road structure can be divided into the asphaltic layer and unbound layer (including the sub-base and sub-grade), as shown in Fig. 4.

To determine the Rayleigh damping parameters, the natural frequencies should be determined first. As the natural frequencies are strongly dependent on the thickness and stiffness modulus of the layers, it assumes very different values for the asphaltic layer and unbound layer. The unbound layer can generally be considered semi-infinite, so the effects from the asphaltic material layer can be almost ignored. Therefore, with simple boundary conditions, the natural frequency of the unbound layer can be directly extracted by the FE method. However, for the asphaltic layer, the support effects from the unbound layer cause complicated boundary conditions that are difficult to apply directly by FE technologies. To solve this problem, the idealized shear beam model proposed by Dobry et al. [56] to estimate the fundamental period of the layered soil is presented. In this model, the pavement multilayer system is transformed into a layered system of linear elastic shear beams, without considering the horizontal length of the different layers, as shown in Fig. 5.

Each shear beam is considered to be homogeneous with the same cross-sectional area and extends indefinitely in all horizontal directions. The support effect of the unbound layer on the asphaltic layer is modeled by a shear spring with consideration of the shear stiffness. The parameters of each layer required for the computation of the natural frequency are including the shear modulus (G), mass density (ρ), shear-wave velocity (c) and the thickness (H), among which the velocity of a shear wave, c is controlled by the shear modulus,

$$c = \sqrt{\frac{G}{\rho}} \tag{7}$$

For the shear beam representing one structure layer in the pavement, an infinitesimal segment section (dy) at y is assumed and the free vibration of the transverse shear is analyzed, as shown in Fig. 6.

The displacement and shear force at the bottom of the infinitesimal segment section are u and Q, respectively, while those at the top are $u + \frac{\partial u}{\partial y} dy$ and$Q + \frac{\partial Q}{\partial y} dy$, respectively. According to Newton's second law,

$$\frac{\partial Q}{\partial y} dy = \rho A \cdot dy \cdot a \tag{8}$$

where A is the shear area; a is the shear acceleration, which can be presented as $\frac{\partial^2 u}{\partial t^2}$ . Since Q can be given as$GA \cdot \frac{\partial u}{\partial y}$, the Equation (8) can be transformed as,

$$\frac{\partial^2 u}{\partial t^2} = c^2 \cdot \frac{\partial^2 u}{\partial y^2} \tag{9}$$

For the case of steady-state resonance, u(y, t) can be expressed as,

$$u(y,t) = U(y)\exp(i\omega t) \tag{10}$$

where U(y) is the modal shape. Substitute Equation (10) into Equation (9), the free vibration equation of the transverse shear in the frequency domain can be given as,

$$\frac{d^2 U(y)}{dy^2} + \frac{\omega^2}{c^2} U(y) = 0 \tag{11}$$

which can be transformed as,

$$U(y) = A\cos\left(\frac{\omega}{c} y\right) + B\sin\left(\frac{\omega}{c} y\right) \tag{12}$$

where ω is the natural frequency. Correspondingly, the modal shapes for the surface layer and base layers in the pavement model can be expressed respectively as,

$$U_1(y) = C_1 \cos\frac{\omega}{c_1} y + D_1 \sin\frac{\omega}{c_1} y \tag{13}$$

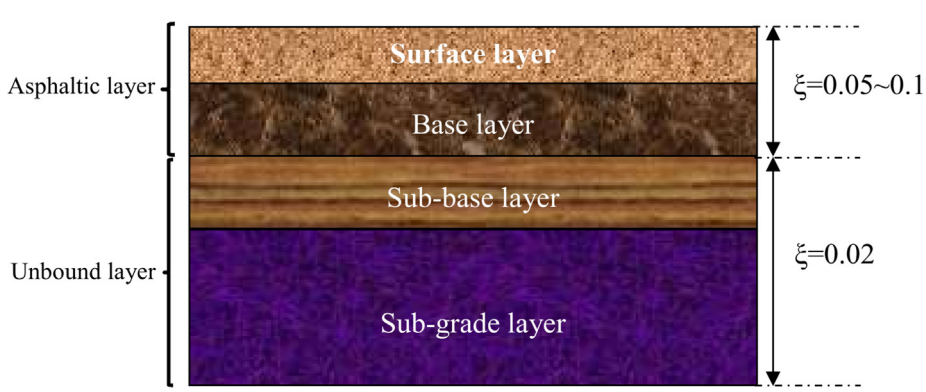


**Fig. 4.** Divisions of the pavement structure.


**Fig. 5.** Shear beam model for pavement.

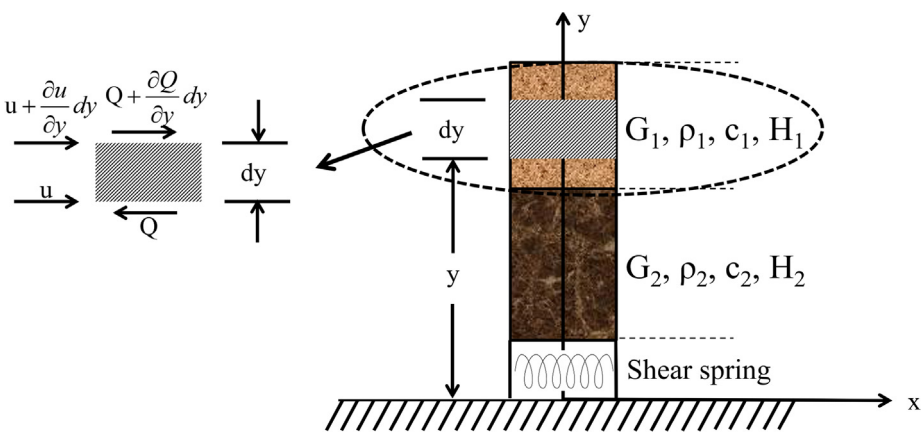


**Fig. 6.** Infinitesimal segment section at y.

$$U_2(y) = C_2\cos\frac{\omega}{c_1}y + D_2\sin\frac{\omega}{c_1}y \tag{14}$$

The natural frequencies can be determined as the solutions of the system composed of these vibration shape functions, taking into account the boundary conditions, which are presented as follows. The free boundary condition at the top of the surface layer can be evaluated as,

$$\frac{dU_1(y)}{dy}\Big|_{y=H_1+H_2} = 0 \tag{15}$$

The stress continuity boundary condition of the bottom of the beam can be given as,

$$G_2A\cdot\frac{dU_2(y)}{dy}\Big|_{x=0} = -K\cdot U_2(y) \tag{16}$$

where K is the shear stiffness of the unbound layer. The stress and displacement continuities at the interface of the surface and base layers are respectively given as,

$$G_1A\frac{dU_1(x)}{dx}\Big|_{x=H_2} = G_2A\frac{dU_2(x)}{dx}\Big|_{x=H_2} \tag{17}$$

$$U_2(H_2) = U_1(H_2) \tag{18}$$

By substituting Equation (13) and Equation (14) to Equations (15), (16), (17) and (18), the implicit solution of the natural frequencies ω can be obtained as follows,

by which the natural frequencies ω of the different modes for the asphaltic layer can be determined, while for those values for the unbound layer, the FE technique can be applied directly for the extract [57]. It should be noted that the obtained solution can be many fitted natural frequencies since each vibration mode should correspond to a natural frequency. However, only the low-order modes of pavement structures tend to be considered in the dynamic analysis.

### 2.2.2. Determining Rayleigh damping parameters

Once the natural frequencies of these sub-layers are determined, the next step is to determine the corresponding Rayleigh damping parameters. As far as these parameters concerned, it can be conjectured that there is a relationship between damping and frequency whilst damping is regarded as mostly frequency independent in a limited frequency range and the small strain material damping is considered as the constant target damping to the form of the Rayleigh damping formulation [55]. Consequently, the Rayleigh damping parameters, α, and β should be appropriately formulated to match the target damping to the modal damping by linear time-domain solutions best.

Most dynamic analyses consider frequency ranges between $\omega_1$ and $\omega_2$, and hence it is very essential to improve the decoupling accuracy in such frequency range [51,53]. In the present study, the method proposed by Song et al. [58] is simplified and applied.

$$\tan\left(\frac{\omega}{c_1}H\right) = \frac{c_2G_1G_2\omega\sin(\frac{\omega}{c_1}H_2) - c_1G_2^2\omega\tan(\frac{\omega}{c_2}H_2)\cos(\frac{\omega}{c_1}H_2) + c_2^2G_1K\tan(\frac{\omega}{c_2}H_2)\sin(\frac{\omega}{c_1}H_2) + c_1G_2Kc_2\cos(\frac{\omega}{c_1}H_2)}{c_2G_1G_2\omega\cos(\frac{\omega}{c_1}H_2) + c_1G_2^2\omega\tan(\frac{\omega}{c_2}H_2)\sin(\frac{\omega}{c_1}H_2) + c_2^2G_1K\tan(\frac{\omega}{c_2}H_2)\cos(\frac{\omega}{c_1}H_2) - c_1G_2Kc_2\sin(\frac{\omega}{c_1}H_2)} \tag{19}$$

In this method, the damping parameters are calculated by the application of the least square method to minimize the difference between the calculated and actual damping ratio of each order within the cut-off frequency, as follows.

$$\min_{\alpha,\beta} \sum_{i=1}^{n} \left( \frac{\alpha}{2\omega_i} + \frac{\beta\omega_i}{2} - \xi \right) \tag{20}$$

However, it should be noted that unlike those large or complex structures, the road pavements tend to be considered more about the low-order modes. Hence, Equation (20) is simplified to reduce the computation as follows. Fig. 7 shows the relationship between Rayleigh damping and frequency.

Assume the differential of Rayleigh damping,

$$\xi = \frac{\alpha}{2\omega} + \frac{\beta\omega}{2} \tag{21}$$

$$\frac{d\xi}{d\omega} = -\frac{\alpha}{2\omega^2} + \frac{\beta}{2} = 0 \tag{22}$$

Then,

$$\omega = \sqrt{\frac{\alpha}{\beta}} \tag{23}$$

Substitute Equation (23) to Equation (21) and the minimum value of the damping ratio, $\xi_{min}$ can be given as,

$$\xi_{min} = \sqrt{\alpha\beta} \tag{24}$$

The damping ratio at the selected frequency range boundary is regarded as the maximum one, which can be expressed as,

$$\xi_{max} = \frac{\alpha}{2\omega_1} + \frac{\beta\omega_1}{2} \tag{25}$$

$$\xi_{max} = \frac{\alpha}{2\omega_2} + \frac{\beta\omega_2}{2} \tag{26}$$

It is worth noting that $\omega_1$ and $\omega_2$ are determined according to the proposed method in the present study. Then, the frequency-independent damping ratio is assumed as,

$$\xi_0 = \frac{1}{2}(\xi_{min} + \xi_{max}) \tag{27}$$

In this way, a closer relationship between the Rayleigh and the frequency-independent damping can be observed in Fig. 5. Besides, only the natural frequencies of the two models are required to be determined, by which the efficiency of the solution is improved under the premise of ensuring the accuracy of the operation.

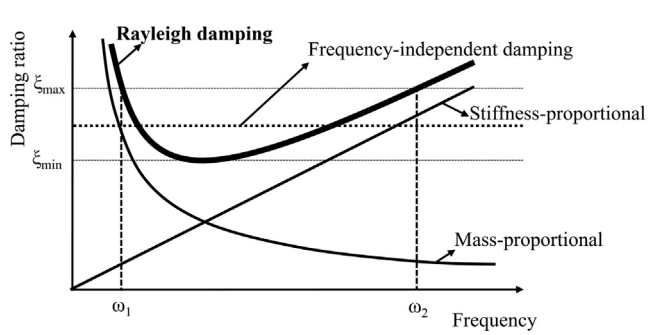


**Fig. 7.** Relationship between damping and frequency by the proposed method.

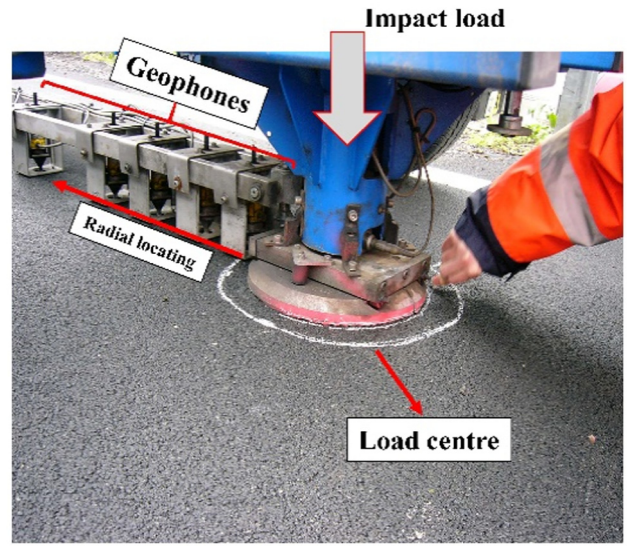


**Fig. 8.** An experimental test of falling weight deflectometer (FWD).

## 3. Field testing and model validation

To evaluate the accuracy of the developed method, a calibration process is conducted. The FE simulation based on the developed method is established to compare the dynamic response with in-situ experimental tests of falling weight deflectometer (FWD), which is a widely used non-destructive test for flexible pavement evaluation and assessment of residual life. The FWD (Fig. 8) applies an impact load to the pavement surface, to simulate the action of traffic, and the pavement response in terms of deflections is measured at several radial locations from the load center. To examine the applicability of the proposed method, the in-situ measurements including non-rubberized and rubberized asphalt pavement were carried out.

### 3.1. Construction of the finite element (FE) model

In the pavement structure, the dynamic analysis can be performed by the following equation in which the damping and inertia effects are presented.

$$[M]\{\ddot{U}\} + [C]\{\dot{U}\} + [K]\{U\} = \{P\} \tag{28}$$

where [M] = mass matrix, [C] = damping matrix, [K] = stiffness matrix, {P} = external force vector, {Ü} = acceleration vector, $\{\dot{U}\}$ = velocity vector, and {U} = displacement vector. In the present

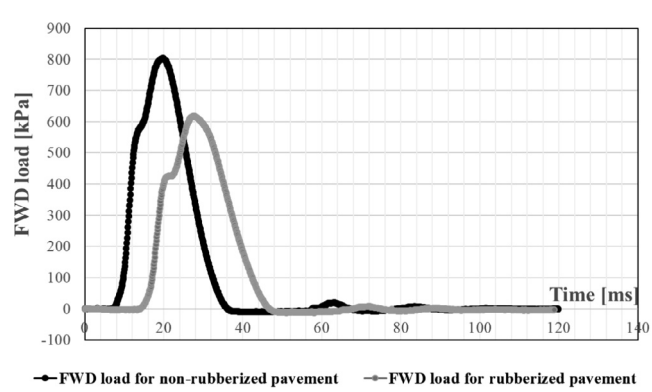


**Fig. 9.** FWD loads for the non-rubberized and rubberized pavements.

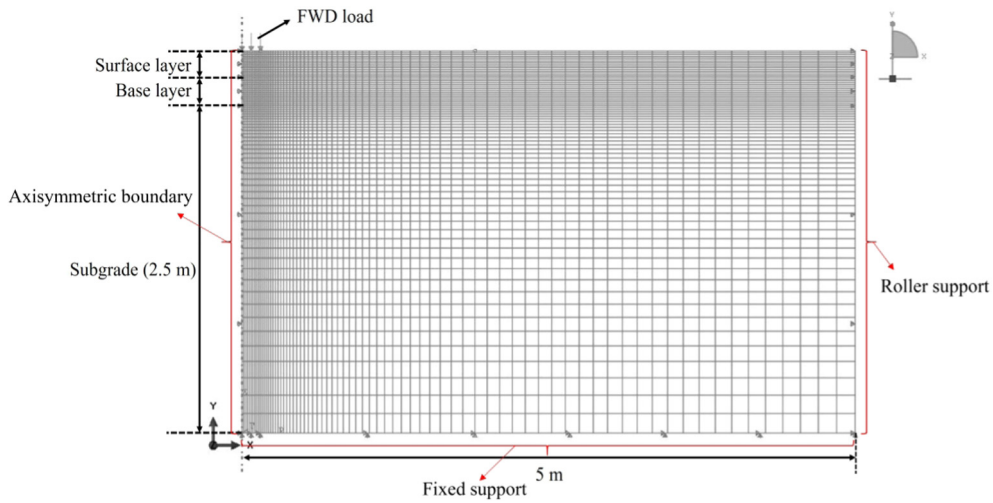


**Fig. 10.** Schematic of the FE model in ABAQUS.

study, the implicit analysis (time-domain) in ABAQUS is selected as the solution for Equation (28) for its stability and efficiency. The same pulse loads (Fig. 9) conducted in the FWD tests of non-rubberized and rubberized pavements are applied in the simulation. The total simulation time equals 120 ms with a step length of 1 ms.

A 2D FE model of the pavement structure is presented in Fig. 10, with the composition of three layers, including an asphaltic surface layer, the sub-base layer, and subgrade, which are homogeneous in horizontal planes. The axisymmetric model by using roller vertical boundary node and fixed supports for the bottom boundary node was employed.

The haversine pulse load is applied on a circular footprint with a radius of 0.15 m and it is the idealized representation of the dynamic loading applied by the passage of traffic, which is also recognized as the load subjected to falling weight deflectometer (FWD) tests. The 4-node bilinear axisymmetric quadrilateral and reduced integration element, CAX4R was selected as a mesh element type in order to improve the calculation accuracy and to reduce calculation time. The FE model was meshed by refining the loading and upper areas as well as roughening the remaining ones. The different grid densities and model sizes were selected in this study to evaluate the influence of these modeling parameters on the accuracy of numerical modeling. The optimized grid and model size was determined based on convergence optimization.

Table 1 gives the properties of the material for the two pavements. The layer moduli, density, and Poisson's ratio are back-calculated from FWD tests and the damping ratios are optimized from the values by Zhong et al. [59]. The calculation for layer moduli was performed by the ELMOD software, separately for the layers thickness data obtained by coring. The corresponding Rayleigh damping parameters were calculated according to the method proposed in the present study. After that, they directly inputted into the damping option of the material behavior in ABAQUS, and the damping behavior of the asphaltic and unbound materials can be defined.

### 3.2. Comparison between the numerical and testing results

The results of FWD testing was used for comparison with numerical results. Fig. 11 gives a detailed description of the experimental setup and measured components.

In this study, 9 geophone sensors consisting of a permanent magnet and a mass with a coil, coupled through spring were employed for the test. A movement of the geophone leads to a relative movement between the coil and magnet due to the inertia of the mass. Proportional to the speed of this relative movement, a voltage is induced in the coil which is used to calculate the speed given an appropriate calibration. The deflection is further determined by integrating the speed. Finally, the deflection basin and the deflection time-history for each sensor were measured and recorded.

Fig. 12 presents the comparison of deflection basin curves for the field measurements and FE simulations.

The FE simulation results of the deflection basin curves are completely overlapping with the field measurement data, while it is worth noting that for model validation, these comparisons can be inadequate because the deflection basin curve cannot fully reflect the characterization of damping since only those maximum deflection values are recorded. Therefore, the deflection history curves of three sensors during the FWD measurements are recorded for each pavement, as shown in Table 2.

These deflection histories from the FWD field measurements are used as benchmarks to validate the accuracy of the proposed method as well. The comparison results are presented in Fig. 13 and Fig. 14.

**Table 1**
Properties of the materials in the pavements.

| Pavements | layers | Thickness [cm] | Young's Modulus [MPa] | Poisson ratio | Damping ratio | Density[Kg/m$^3$] |
|---|---|---|---|---|---|---|
| Non-rubberized pavement | Surface layer | 20.5 | 5680 | 0.3 | 0.05 | 2400 |
| | Base layer | 22.5 | 660 | 0.3 | 0.03 | 2000 |
| | Subgrade | – | 110 | 0.35 | 0.03 | 1500 |
| Rubberized pavement | Surface layer | 20.4 | 2657 | 0.3 | 0.1 | 2400 |
| | Base layer | 29.2 | 73 | 0.3 | 0.03 | 2000 |
| | Subgrade | – | 66 | 0.35 | 0.03 | 1500 |

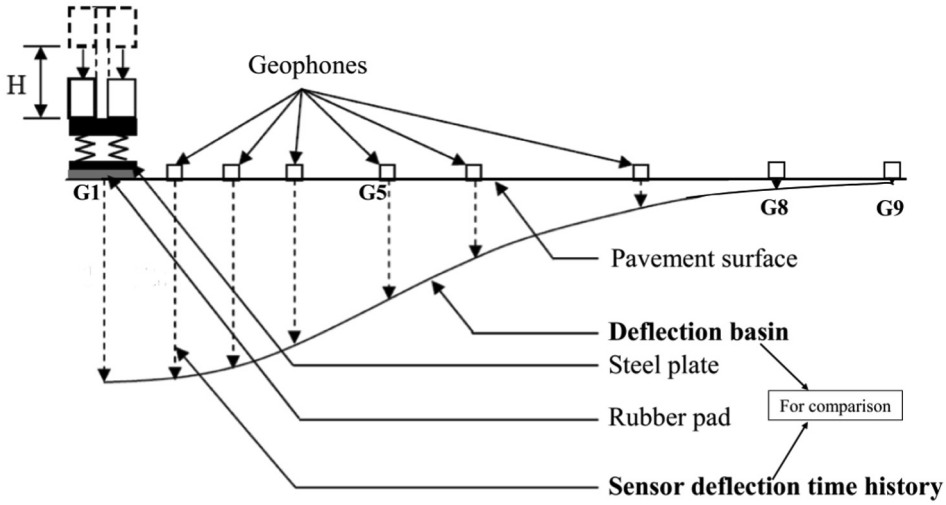


**Fig. 11.** Experimental setup and measured components.

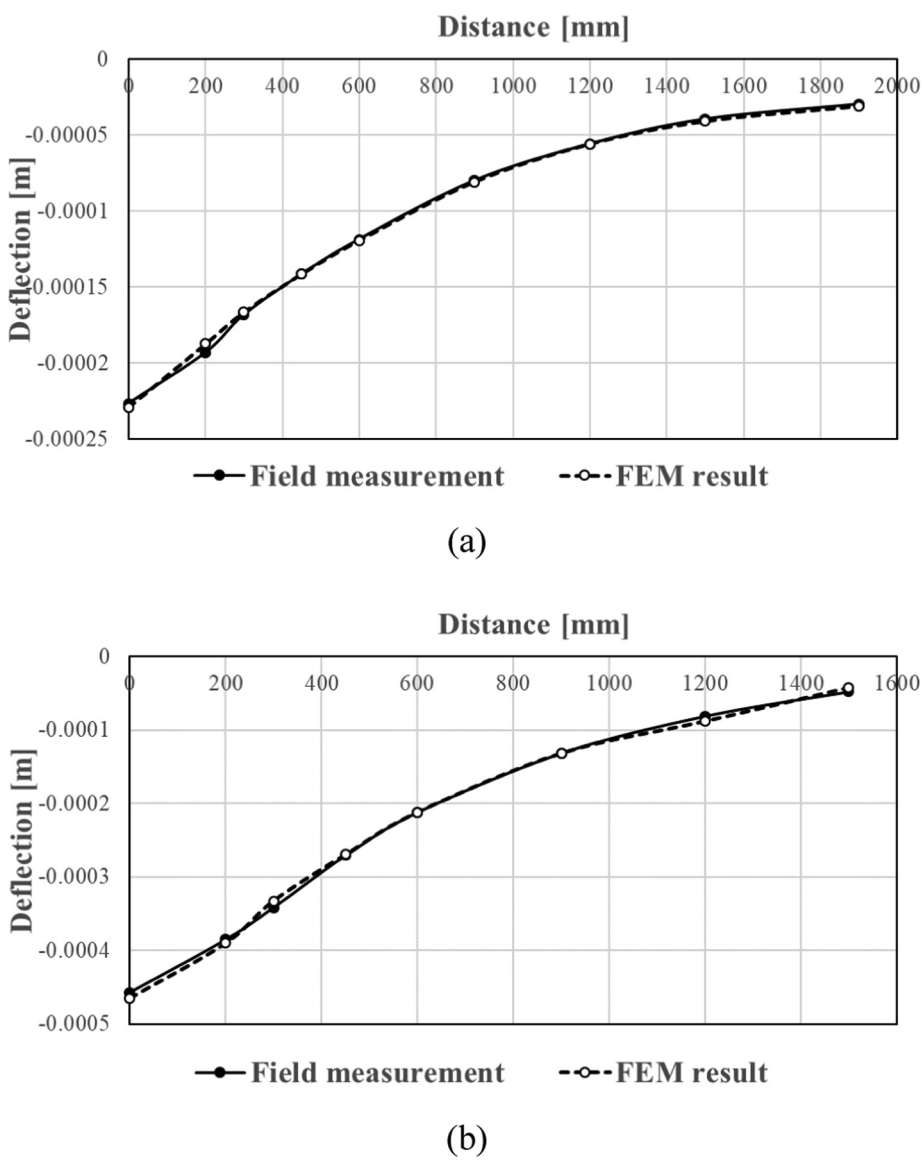


**Fig. 12.** Comparison of deflection basin curves for the field measurements and FE simulations: (a) Non-rubberized pavement; (b) Rubberized pavement.

**Table 2**
Sensors to record the deflection history in each pavement.

| | | | | |
|---|---|---|---|---|
| Non-rubberized pavement | Measurement points | Sensor G1 | Sensor G5 | Sensor G9 |
| | Distance from the FWD load [mm] | 0 | 500 | 1900 |
| Rubberized pavement | Measurement points | Sensor G1 | Sensor G5 | Sensor G8 |
| | Distance from the FWD load [mm] | 0 | 500 | 1500 |

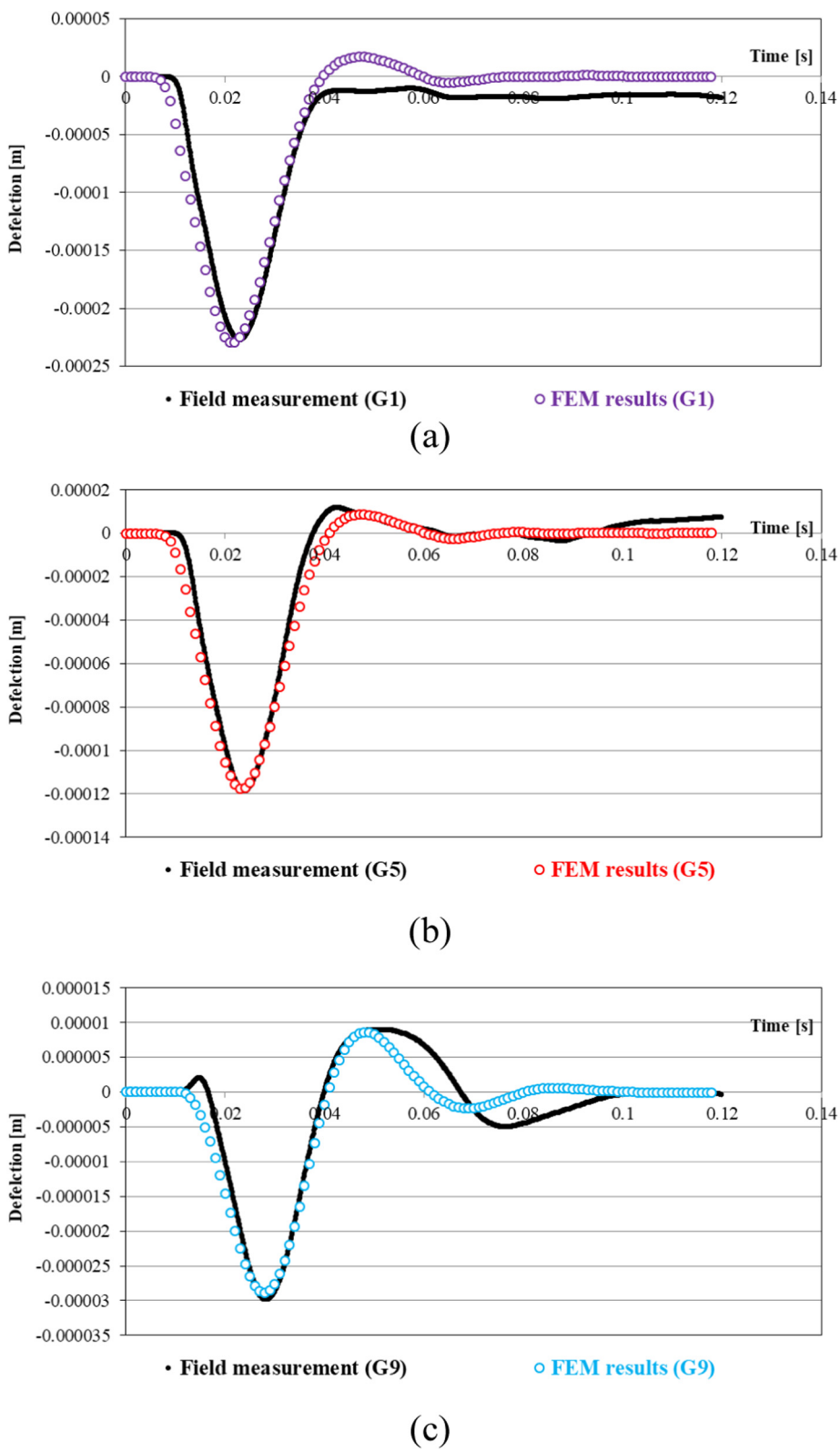


**Fig. 13.** Comparisons of the non-rubberized pavement at different points: (a) G1; (b) G5; (c) G9.

As far as the non-rubberized pavement, except for a small magnitude difference at G1 and dephasing at G9, good agreements are achieved. The magnitude difference at G1 can be explained by the falling weight which impedes the vibration at the loading point. Theoretically speaking, the deflection history should be a vibration curve along with the pavement-air interface similar to the FE simulation result. For the dephasing at G9, it can be influenced by the heterogeneity of the subgrade, since G9 is the furthest point from the load. Similarly, good agreements of amplitudes and phases can be observed for the rubberized pavement except for the magnitude difference at G8 due to the non-homogeneity of the ground. In any case, these differences are considered acceptable for the developed method. Besides, the proposed method for calculating the Rayleigh damping parameters is not only applicable to the conventional non-rubberized pavements, but also to those rubberized ones.

## 4. Parametrical studies for the anti-vibration pavement

### 4.1. FEM simulations of the vibration reduction

Similar to the model establishing process mentioned above, the anti-vibration pavement with the damping layer was simulated, as presented in Fig. 15.

The simulation represents a cross-section of a typical pavement structure with the surrounding environment. The pavement structure consists of an asphalt concrete (AC) layer, a layer of subbase, and a layer of subgrade by the compacted soil and the surrounding environment characterized by the un-compacted soil. The mechanical properties of the materials for the pavements and surrounding environment are listed in Table 3.

The thickness, elastic modulus, and Poisson ratio of each layer are back-calculated from the field FWD tests while the elastic modulus of the damping layer is determined according to the laboratory results by the means of dynamic modulus evaluation (AASHTO TP 79-12).

The damping layer is placed at 0, 5 cm, 10 cm, 15 cm, and 20 cm from the top to evaluate the effect of damping layer position on vibration attenuation. The effect of the damping thickness is evaluated with values of 0, 1, 2, and 3 cm. The damping ratio of the damping layer varies by 0.02, 0.05, 0.1, 0.15, and 0.2. The magnitude of the load is determined as 800 kPa, representing the axle loading of the passing traffic. Five points including point A, on the pavement directly underneath the loading and point B, C, D, and E, which are 2, 4, 10, and 30 m away from the loading, were monitored for their time histories of accelerations during the simulations. The root-mean-square acceleration ($A_{RMS}$) was recorded at the five monitored points closely for evaluation of vibration reduction and it is given by

$$A_{RMS} = \sqrt{\frac{1}{T}\int_0^T a^2(t)dt} \tag{29}$$

where a(t) is the acceleration at time t, and T is the duration of vibration. The RMS refers to a common mathematical method of defining the effective magnitude. For a uniform sine wave, the root-mean-square value is 0.707 times the peak value or 0.354 times the peak-to-peak value. By comparing the root-mean-square and peak accelerations of monitored points, the capacity of the damping layer in the vibration reduction can then be determined [47,60].

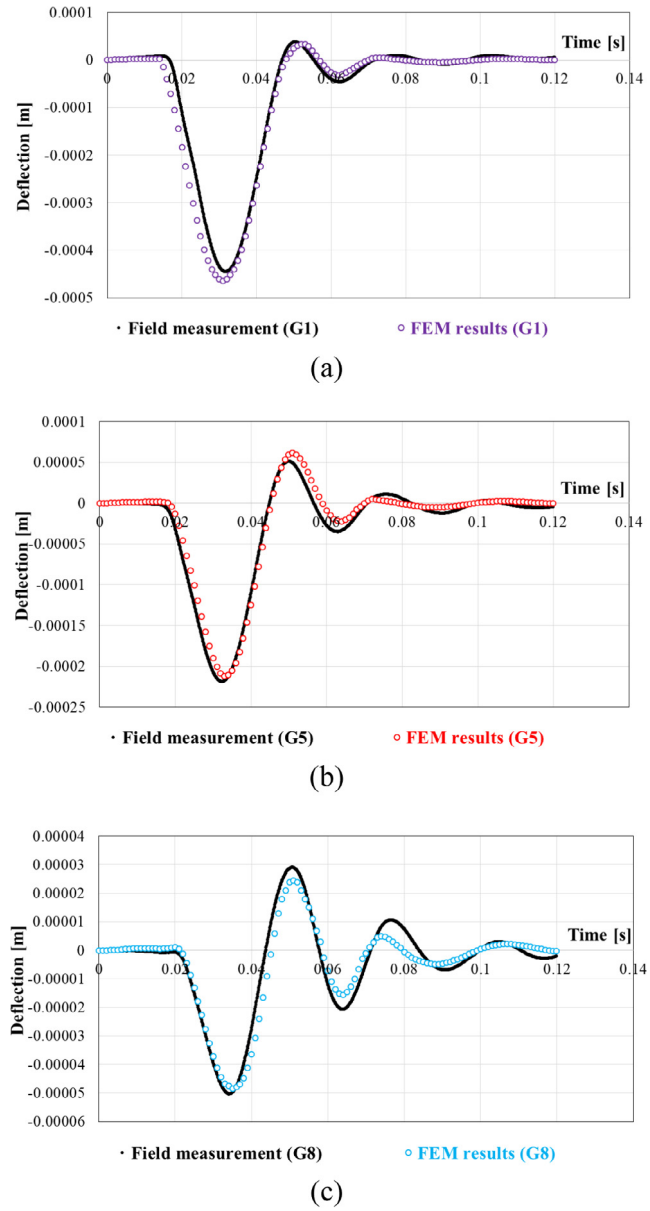


**Fig. 14.** Comparisons of the rubberized pavement at different points: (a) G1; (b) G5; (c) G8.

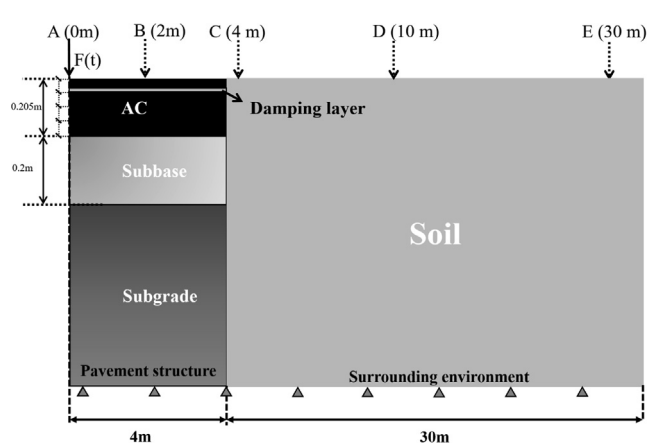


**Fig. 15.** Schematic diagram of the finite-element simulation.

**Table 3**
Mechanical properties used for the FE simulations.

| Structures | | Materials | Thickness [cm] | Elastic modulus [MPa] | Poisson ratio | Damping ratio | Density[Kg/m$^3$] |
|---|---|---|---|---|---|---|---|
| Pavement | Surface layer | Asphalt concrete (AC) | 20.5 | 5680 | 0.3 | 0.05 | 2400 |
| | Subbase layer | Gravel stones (GS) | 22.5 | 660 | 0.3 | 0.02 | 2000 |
| | Subgrade | Compacted soil | – | 110 | 0.35 | 0.02 | 1500 |
| Damping layer | | DAMs | 0, 1, 2, 3 | 850 | 0.3 | 0.02, 0.05, 0.1, 0.15, 0.2 | 2400 |
| Surrounding environment | | Un-compacted soil | – | 110 | 0.35 | 0.02 | 1500 |

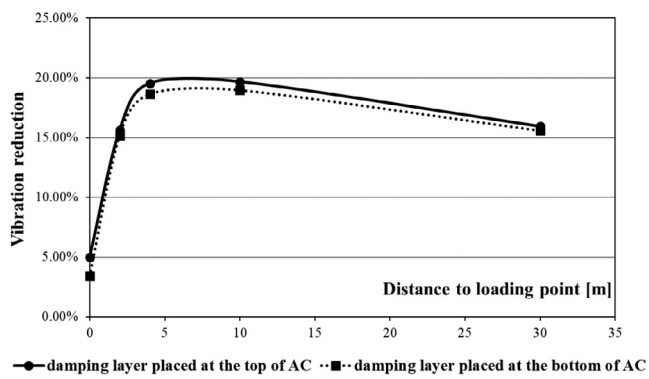


**Fig. 16.** Relationship between the monitored points and vibration reduction.

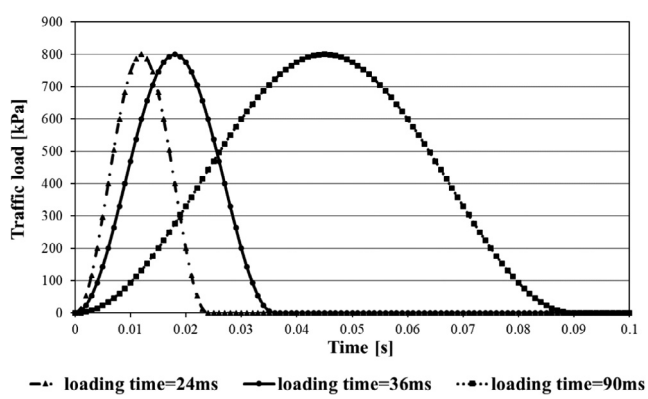


**Fig. 17.** Loads applied in the simulations.

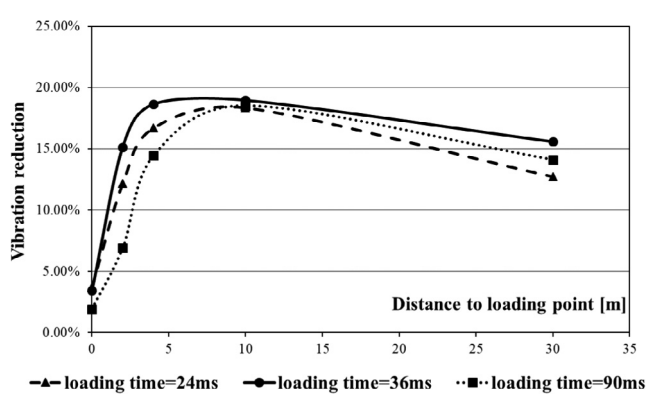


**Fig. 18.** Sensitive analysis for varying traffic loads.

## 4.2. Results of parametrical studies

### 4.2.1. Sensitive analysis of varying monitored points

As the damping layer with a thickness of 30 mm is at the bottom and top of the asphalt concrete (AC) layer, the influences of

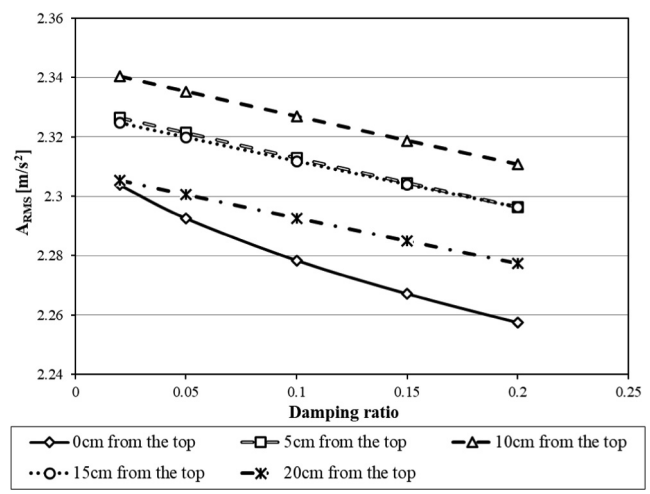


**Fig. 19.** Effects of the damping ratio on vibration reduction (at monitored point A; damping layer thickness = 10 mm).

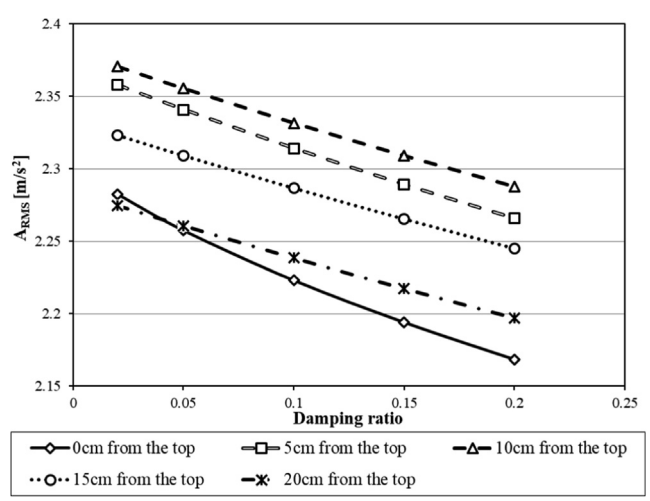


**Fig. 20.** Effects of the damping ratio on vibration reduction (at monitored point A; damping layer thickness = 30 mm).

varying monitored points on vibration reduction were evaluated. The vibration reduction was determined as follows. As the damping ratio of the damping layer change from 0.02 to 0.2, the $A_{RMS}$ at the monitored point are recorded as $A_{RMS}$ ($\xi = 0.02$) and $A_{RMS}$ ($\xi = 0.2$), respectively. Then the vibration reduction, $\Delta_{vibration}$ can be presented as,

$$\Delta_{vibration} = \frac{A_{RMS}(\xi = 0.02) - A_{RMS}(\xi = 0.2)}{A_{RMS}(\xi = 0.02)} \tag{30}$$

by which the $\Delta_{vibration}$ at the five monitored points A, B, C, D, and E are recorded. Fig. 16 presents the relationship between distance (from the monitored point to the loading point) and $\Delta_{vibration}$ as the damping layer is placed at the top and bottom of the AC, respectively.

A relative higher vibration reduction, 15% is observed when the monitored point is approximately 2 m to 30 m away from the loading point. As the increase of the distance, the vibration reduction increases firstly and then decreases. The maximum value appears at a distance of 5–6 m. Also, regardless of the damping layer is at the top or the bottom of the asphalt layer, similar results can be obtained. As the loading point is regarded as the monitored point, the minimum vibration reduction appears.

The loading point is on the pavement, where the vibration response much depends on the stiffness and mass characteristics instead of the damping characteristics. The damping ratio changes from 0.02 to 0.2 while the other parameters related to the stiffness and mass characteristics stay the same. Hence, minor displacement and phase difference can be obtained, resulting in a minor reduction of $A_{RMS}$. When the distance from the monitored point to the loading point increases, the damping effect of the damping layer plays a predominant role thus the gradually obvious reduction of $A_{RMS}$ can be found. However, with the continuous increase in distance, the damping effect of the surrounding soil starts to play the predominant role, causing the reduction of $\Delta_{vibration}$. It can be predicted when the distance is far enough, the $\Delta_{vibration}$ may decrease until it vanishes.

*4.2.2. Sensitive analysis of varying traffic loads*

As a special dynamic structure, the pavement may vibrate differently with varying loads. To evaluate the sensitivity of varying loads, three haversine pulse loads (Fig. 17) with loading times of 24 ms, 36 ms, and 96 ms are applied.

As the damping layer is located at the bottom of the AC layer, the results of vibration reduction for varying loads are presented in Fig. 18.

For different loading times, the maximum vibration reduction appears at different distances. For the loading time of 36 ms, the maximum vibration reduction is observed at 5 m away from the loading point and a relatively higher $\Delta_{vibration}$ can be obtained; while for the loading times of 24 ms and 90 ms, the maximum vibration reductions appear at approximate 10 m away from the loading point. However, in any case, the three loads show very similar trends, demonstrating that the dynamic response of the anti-vibration pavement is not sensitive to the pulse loads with varying loading times.

*4.2.3. Effect of damping ratio of the damping layer*

Five damping ratios were selected to determine their effects on vibration reduction. The $A_{RMS}$ (as the damping layer thickness is 10 mm) at monitored point A with varying damping ratios are presented in Fig. 19, where varying damping layer positions are given in the legend part.

As the increase of the damping ratio, the $A_{RMS}$ decrease with obvious linearity. This may be explained that, compared to other layers (AC layer, subbase layer) and subgrade, the damping layer plays a predominant role in characterizing the damping of the whole system, causing the $\Delta_{vibration}$ of the whole system strong linearity with the damping ratio. Fig. 20 presents the simulation results of the $A_{RMS}$ at point A when the damping layer thickness is 30 mm.

Similar results are obtained compared to those obtained when the thickness is 10 mm, demonstrating the linear reduction of $A_{RMS}$ can still be applicable for different damping layer thickness. In such a linear relationship, the slope of the $A_{RMS}$ curve represents the effect of varying damping ratios. A higher slope value, demonstrating the more obvious effect of vibration reduction, is more preferable during the process of optimizing the damping ratio. However, all the $A_{RMS}$ show closed slope values, though a little higher slope value when the damping layer is 0 cm from the top, by which bare practical significance can be supported.

Fig. 21 and Fig. 22 are the effects of damping ratios at point E when the damping layer thicknesses are 10 mm and 30 mm, respectively.

A similar linear relationship between damping ratio and $A_{RMS}$ can also be found at monitored point E. When the damping layer thickness is 30 mm and the damping ratio changes from 0.02 to 0.2, the vibration at 10 m and 30 m away from the pavement can reduce about 20% and 15%, respectively. Such reductions can demonstrate the significant benefits of the damping layer in reducing the impact of traffic-induced vibrations on the surrounding environment and building.

The damping property of the asphaltic material is highly dependent upon the environmental conditions to which they are exposed. As loading time and temperatures change, the damping ratio will vary even if the same boundary condition. However, according to the viscoelastic property of the asphaltic materials, the intrinsic material damping at the same condition of temperature, load, and boundary condition can be roughly compared. Particularly, for the pavement structure with normal temperature and load, the damping ratios of soil, conventional asphalt mix, and rubberized asphalt mixture can be regarded as 0.02, 0.05, and 0.1, respectively. Hence, to obtain the obvious vibration reduction effect, the damping ratio of the high-damping mix asphalt special for the damping layer should arrive at 0.15–0.2, which is almost

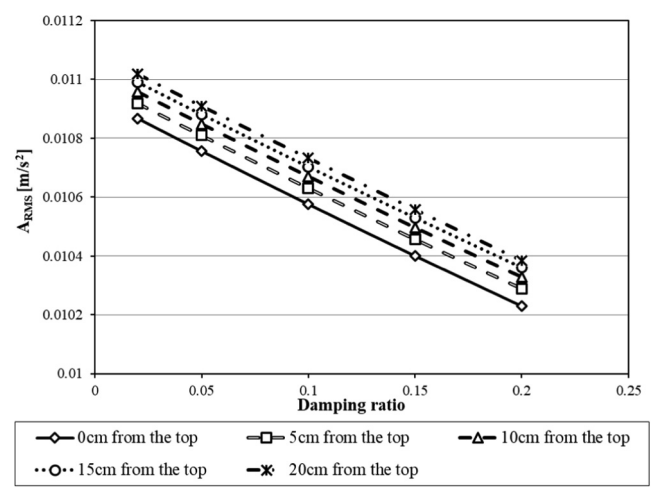


**Fig. 21.** Effects of the damping ratio on vibration reduction (at monitored point E; damping layer thickness = 10 mm).

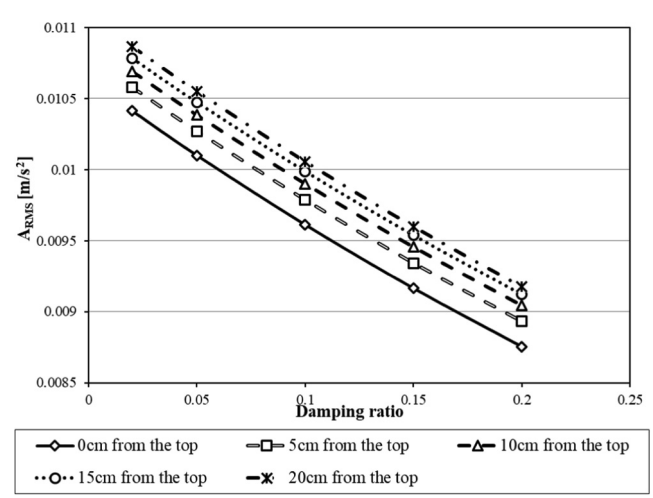


**Fig. 22.** Effects of the damping ratio on vibration reduction (at monitored point E; damping layer thickness = 30 mm).

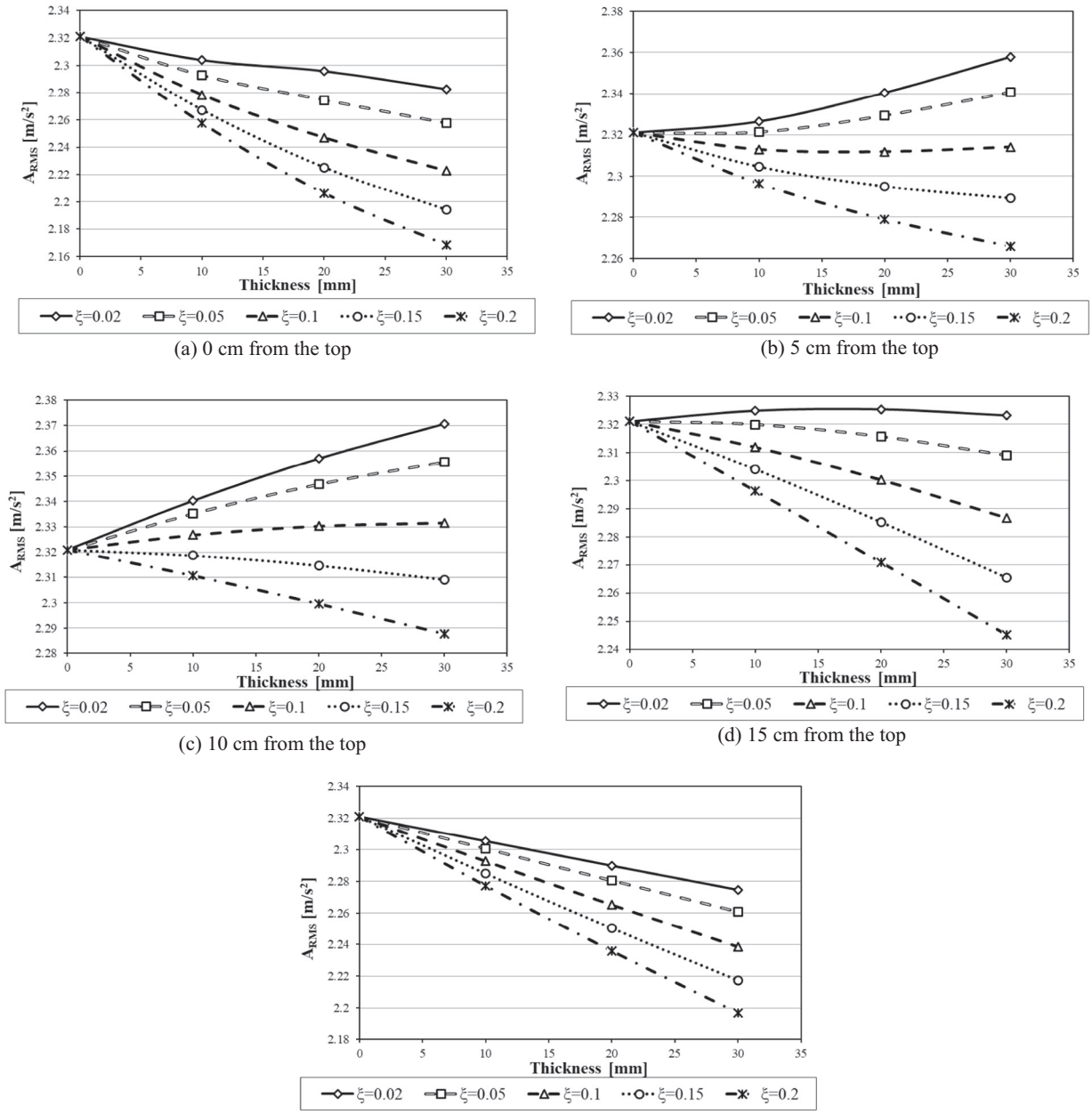


(a) 0 cm from the top

(b) 5 cm from the top

(c) 10 cm from the top

(d) 15 cm from the top

(e) 20 cm from the top

**Fig. 23.** Effects of damping thickness at monitored point A.

2 times compared to conventional rubberized mix under the same loading condition, while from the laboratory results obtained, such design target has already arrived.

### 4.2.4. Effect of the damping layer thickness

Another very essential design parameter for the anti-vibration pavement is the damping layer thickness. In this series of simulations, the thickness of the damping layer was varied from 0 mm, 10 mm, 20 mm to 30 mm. The effect of damping layer thickness at monitored point A is shown in Fig. 23.

The increasing thickness of the damping layer does not necessarily reduce the vibration response at point A. For example, as the damping layer is 5 cm from the top, with the increased thickness, the vibration can show the trend of increase for $\xi = 0.02$ or 0.05, demonstrating that the increasing thickness of the damping layer may have a negative effect as the damping ratio is low. This can be due to the lower elastic modulus of the high-damping asphalt mixtures, composed by which the thicker layer can result in a higher vibration under the same load. However, such a negative effect can occur only when the monitoring point is point A. Considering the vibration reductions at monitored points E (see Fig. 24), positive effects caused by the increased thickness can always be found.

Besides, the reductions are almost linear for all thicknesses, from which the optimized thickness of the damping layer cannot be obtained directly. However, based on the consideration of construction cost and pavement structure reliability, 30 mm can be regarded as the optimized thickness.

### 4.2.5. Effect of the damping layer position

When the thickness of the damping layer is 30 mm, the effects of the damping layer position on $A_{RMS}$ at monitored points A, C, and E are evaluated, as shown in Fig. 25. The horizontal axis represents the damping layer position, which is the distance from the top.

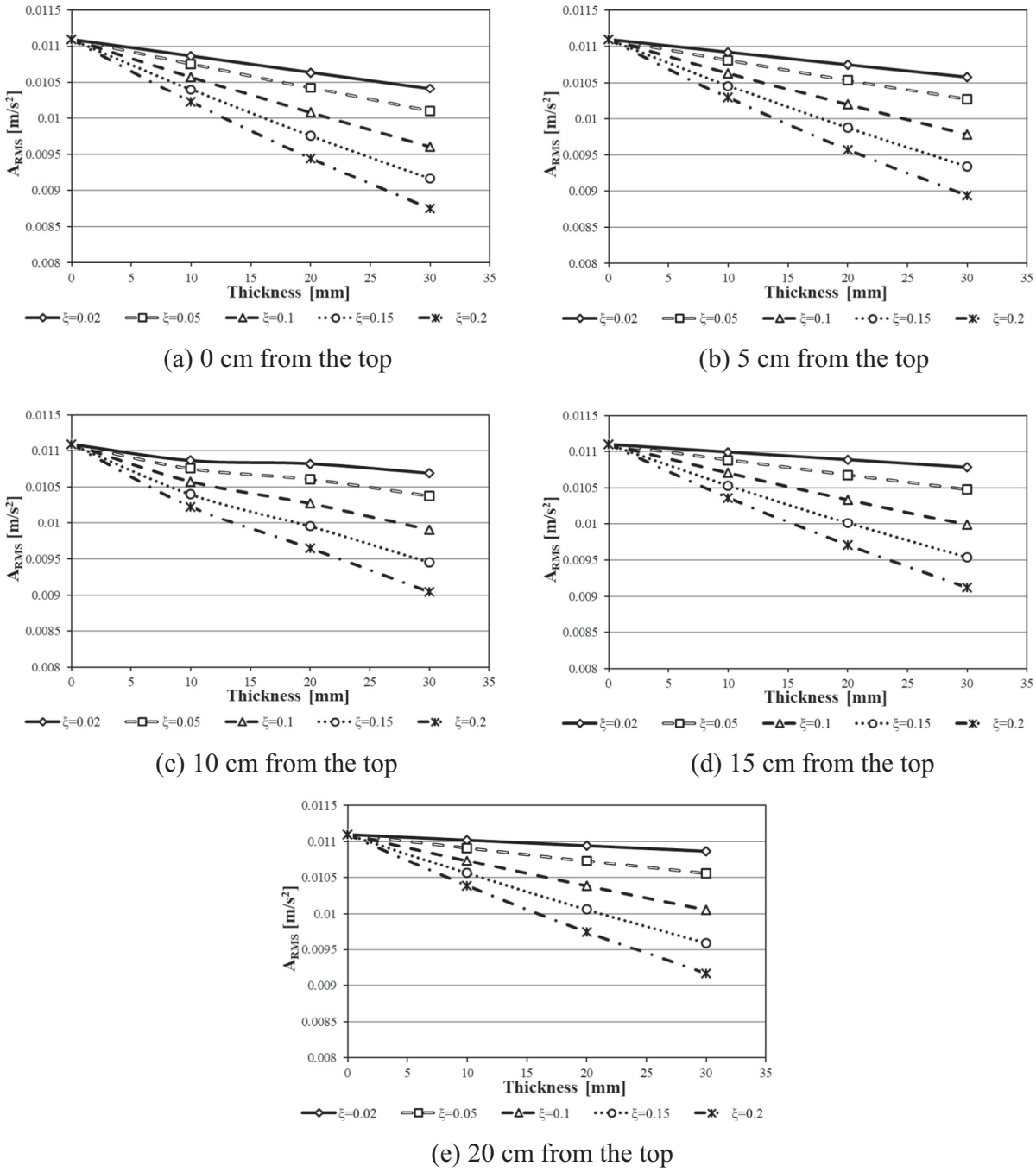


**Fig. 24.** Effects of damping thickness at monitored point E.

The varying damping layer positions have a relatively obvious effect at point E compared to point C and point A; at point C, changing the position of the damping layer has almost no effect on the vibration response of the system. Hence, it can be concluded that the most meaningful point to select the optimized damping layer position is point E, where the values of $A_{RMS}$ the damping layer placed at the top is the optimal position. However, due to the low indirect tensile strength (ITS) evaluated from the laboratory tests [17–19,61], the damping layer cannot work as a surface layer and the second choice might be the optimized position. Hence, it is determined that the optimized position for the damping layer can be 5 cm or 10 cm from the top.

## 5. Conclusions

To reduce traffic-induced vibrations, a novel trial pavement by the anti-vibration technology with a special damping layer was developed. To more fully examine the effectiveness of such a damping layer in the application and optimize the pavement structure, a novel method to determine the two parameters of the Rayleigh damping for the dynamic modeling was proposed. The numerical simulations based on a two-dimensional (2D) finite element (FE) model of the anti-vibration pavement were conducted. The conclusions from the present study can be highlighted as:

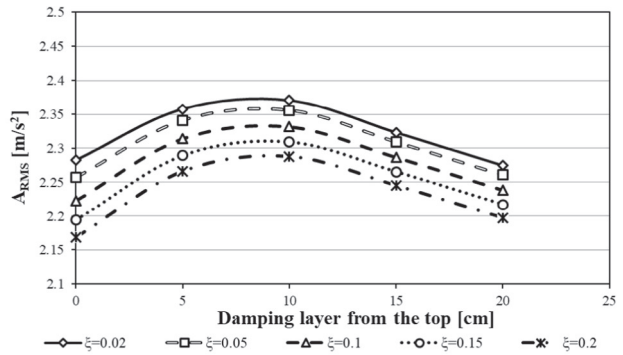


(a) Point A

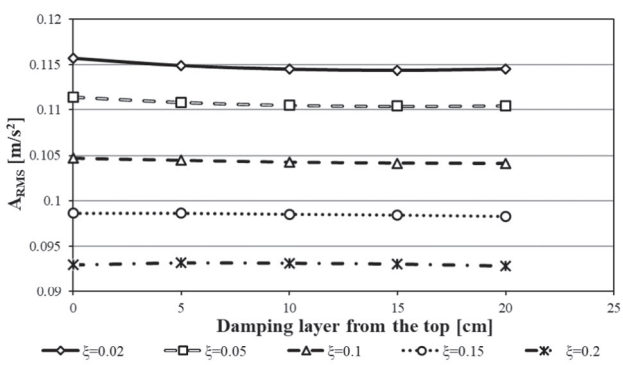


(a) Point C

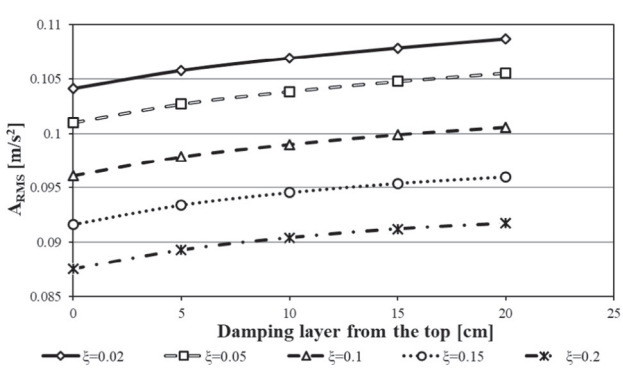


(C) Point E

**Fig. 25.** Effects of damping layer position on vibration reduction.

- Based on the idealized shear beam model, a more reasonable method to calculate natural frequencies of different layers in the flexible pavement was proposed, by which the global damping matrix of the road pavements can be assembled.
- The least-squares method was simplified and used to calculate the frequency-independent damping to reduce the computation. The best-fit Rayleigh damping was obtained by only determining the natural frequencies of the two models. FE model and in-situ field experimental subjected the same FWD pulse loads are performed to validate the accuracy of this method. Good agreements are noted between simulation and field in-situ results demonstrating that this method can provide a more accurate prediction of the vibration response for flexible pavement.
- Sensitivity analysis of varying monitored points and varying loads showed that, by laying a damping layer in the pavement structure, the obvious vibration reduction of 15%∼20% can be observed from 2 m to 30 m away from the loading point. Such results can demonstrate the effectiveness of the damping layer on the pavement and the surrounding environment. For the loads with different loading times, the maximum vibration reductions can appear at different distances but show very similar trends, demonstrating the low sensitivity of the pavement structure on the loads.
- With the increase of damping ratio, the $A_{RMS}$ at the monitored point decreases linearity. To obtain the obvious effect of vibration-reduction, the damping ratio of the materials special for the damping layer should arrive at 0.15–0.2, which is almost 2 times compared to conventional rubberized mix under the same loading condition, while from the laboratory results obtained, such design target can be realized.
- The increasing thickness of the damping layer does not necessarily reduce the vibration response at point A due to the low elastic modulus of damping asphalt mixtures (DAMs); while considering the vibration reductions at monitored points C and E, positive effects caused by the increased thickness can always be found. Based on the construction cost and structure reliability, 30 mm can be the optimized thickness for the damping layer.
- The effects of varying damping layer position at point A and E have a relatively more obvious effect compared to point C. For the pavement structure referred to in the present study, the optimized position for the damping layer is 5 cm or 10 cm away from the top.

## CRediT authorship contribution statement

**Jiandong Huang:** Conceptualization, Methodology, Validation, Formal analysis, Investigation, Resources, Data curation, Writing - original draft. **Massimo Losa:** Writing - review & editing, Project administration, Funding acquisition, Supervision. **Pietro Leandri:** Writing - review & editing, Project administration, Supervision. **Shiva G. Kumar:** Validation, Writing - original draft. **Junfei Zhang:** Methodology, Validation. **Yuantian Sun:** Validation, Investigation, Data curation, Writing - original draft, Writing - review & editing.

## Declaration of Competing Interest

The authors declare that they have no known competing financial interests or personal relationships that could have appeared to influence the work reported in this paper.

## Acknowledgment

The authors sincerely acknowledge the support from the Faculty Start-up Grant of China University of Mining and Technology (Grant No. 102520282) and the assistance of the road engineering lab of the University of Pisa for the field testing.

## References

[1] M. Browne, J. Allen, T. Nemoto, D. Patier, J. Visser, Reducing social and environmental impacts of urban freight transport: A review of some major cities, Procedia-Soc. Behav. Sci. 39 (2012) 19–33.
[2] P. Clemente, D. Rinaldis, Protection of a monumental building against traffic-induced vibrations, Soil Dyn. Earthquake Eng. 17 (5) (1998) 289–296, https://doi.org/10.1016/S0267-7261(98)00012-8.
[3] O. Hunaidi, M. Tremblay, Traffic-induced building vibrations in Montréal, Can. J. Civ. Eng. 24 (5) (1997) 736–753, https://doi.org/10.1139/l97-023.
[4] D. Ouis, Annoyance from road traffic noise: A review, J. Environ. Psychol. 21 (1) (2001) 101–120, https://doi.org/10.1006/jevp.2000.0187.
[5] H. Hao, T. Ang, J. Shen, Building vibration to traffic-induced ground motion, Build. Environ. 36 (2001) 321–336.
[6] O. Hunaidi. Traffic vibrations in buildings. Citeseer: 2000.
[7] S.-H. Ju, Finite element investigation of traffic induced vibrations, J. Sound Vib. 321 (3-5) (2009) 837–853, https://doi.org/10.1016/j.jsv.2008.10.031.

[8] J. Huang, Y. Sun. Effect of modifiers on the rutting, moisture-induced damage, and workability properties of hot mix asphalt mixtures. Appl. Sci. 2020, 10, 7145.
[9] J. Huang, M. Losa, P. Leandri. In Determining the effect of damping layers in flexible pavements on traffic induced vibrations, Advances in Materials and Pavement Prediction: Papers from the International Conference on Advances in Materials and Pavement Performance Prediction (AM3P 2018), April 16-18, 2018, Doha, Qatar, 2018; CRC Press: p 255.
[10] U. Sandberg, Low noise road surfaces. A state-of-the-art review., J. Acoust. Soc. Jpn (E) 20 (1) (1999) 1–17, https://doi.org/10.1250/ast.20.1.
[11] U. Sandberg, The Global Experience in Using Low-Noise Road Surfaces: A Benchmark Report, Hong Kong Environmental Protection Department, Hong Kong, 2009.
[12] L. Venturini, F. Giannattasio, L. Sangalli. Anti-vibration pavement: Case of study novara municipality.
[13] G. Dondi, A. Simone. In Soluzioni tecniche innovative per la mitigazione del rumore e delle vibrazioni da traffico stradale, Atti della Conferenza Nazionale sulla politica energetica in Italia.–Università di Bologna–18-19 Aprile, 2005.
[14] F. Grandi. La progettazione di pavimentazioni antivibranti. alma, 2008.
[15] M. Diependaele, L. Rens. Continuously reinforced concrete pavement for combined tram-busway in gent, belgium.
[16] J. Huang, Rubber Modified Asphalt Pavement Layer for Noise and Vibration Absorption, University of Florence, Florence, 2019.
[17] J. Huang, Y. Sun, Viscoelastic analysis of the damping asphalt mixtures (dams) made with a high content of asphalt rubber (ar), Adv. Civ. Eng. 2020 (2020) 1–12.
[18] J. Huang, J. Zhang, J. Ren, H. Chen, Anti-rutting performance of the damping asphalt mixtures (dams) made with a high content of asphalt rubber (ar), Constr. Build. Mater. 271 (2021) 121878.
[19] J. Huang, G. Cuciniello, P. Leandri, M. Losa. In Design of rubberized asphalt mixtures for noise and vibration damping layers, Advances in Materials and Pavement Performance Prediction II: Contributions to the 2nd International Conference on Advances in Materials and Pavement Performance Prediction (AM3P 2020), 27-29 May, 2020, San Antonio, TX, USA, 2020; CRC Press: p 269.
[20] T.G. Davies, M.S. Mamlouk, Theoretical response of multilayer pavement systems to dynamic nondestructive testing, Transp. Res. Rec. 1022 (1985) 1–7.
[21] A. Hamim, N.I.M. Yusoff, H. Ceylan, S.A.P. Rosyidi, A. El-Shafie, Comparative study on using static and dynamic finite element models to develop fwd measurement on flexible pavement structures, Constr. Build. Mater. 176 (2018) 583–592.
[22] R. Siddharthan, G.M. Norris, J.A. Epps, Use of fwd data for pavement material characterization and performance, J. Transp. Eng. 117 (1991) 660–678.
[23] A.K. Chopra, Dynamics of Structures: Theory and Applications to Earthquake Engineering, Prentice Hall Inc., Upper Saddle River, NJ, 1995.
[24] A. Feriani, F. Perotti, The formation of viscous damping matrices for the dynamic analysis of mdof systems, Earthquake Eng. Struct. Dyn. 25 (1996) 689–709.
[25] C.-M. Kuo, T.-Y. Tsai, Significance of subgrade damping on structural evaluation of pavements, Road Mater. Pave. Des. 15 (2014) 455–464.
[26] K.-J. Bathe. Finite element procedures. Klaus-Jurgen Bathe: 2006.
[27] J.A. Inaudi, J.M. Kelly, Linear hysteretic damping and the hilbert transform, J. Eng. Mech. 121 (1995) 626–632.
[28] P. Michaels. Water, inertial damping, and the complex shear modulus. In Geotechnical earthquake engineering and soil dynamics iv, 2008; pp 1-10.
[29] C. Phillips, Y.M. Hashash, A simplified constitutive model to simultaneously match modulus reduction and damping soil curves for nonlinear site response analysis, Geotechn. Earthq. Eng. Soil Dyn. iv (2008) 1–10.
[30] J. Wang, X. Zeng, D. Gasparini, Dynamic response of high-speed rail foundations using linear hysteretic damping and frequency domain substructuring, Soil Dyn. Earthquake Eng. 28 (2008) 258–276.
[31] P.A. Zinoviev, Y.N. Ermakov, Energy Dissipation in Composite Materials, CRC Press, 1994.
[32] J. Huang, T. Duan, Y. Zhang, J. Liu, J. Zhang, Y. Lei, Predicting the permeability of pervious concrete based on the beetle antennae search algorithm and random forest model, Adv. Civ. Eng. 2020 (2020) 8863181.
[33] L. Bergman, A. Hannibal, An alternate approach to modal damping as applied to seismic-sensitive equipment, Shock Vib. Bull. 46 (1976) 69–82.
[34] A.W. Bishop, The use of the slip circle in the stability analysis of slopes, Geotechnique 5 (1955) 7–17.
[35] B.J. Lazan. Damping of materials and members in structural mechanics. PERGAMON PRESS LTD, OXFORD, ENGLAND. 1968, 317 1968.
[36] E.E. Ungar, Vibration Isolation, John Wiley & Sons Inc, New York, NY, 1992.
[37] J. Ren, C. Yin, Investigating mechanical characteristics of aggregate structure for road materials, Int. J. Pavement Eng. (2020) 1–15.
[38] J. Ren, B. Xue, L. Zhang, W. Liu, D. Li, Y. Xu, Characterization and prediction of rutting resistance of rock asphalt mixture under the coupling effect of water and high-temperature, Constr. Build. Mater. 254 (2020) 119316.
[39] I.L. Al-Qadi, H. Wang, P.J. Yoo, S.H. Dessouky, Dynamic analysis and in situ validation of perpetual pavement response to vehicular loading, Transp. Res. Rec. 2087 (2008) 29–39.
[40] W. Uddin, S. Garza. 3d-fe simulation study of structural response analysis for pavement-subgrade systems subjected to dynamic loads. In Pavements and materials: Testing and modeling in multiple length scales, 2010; pp 170-181.
[41] I. Chowdhury, S.P. Dasgupta, Computation of rayleigh damping coefficients for large systems, Electron. J. Geotech. Eng. 8 (2003) 1–11.
[42] S.H. Ju, S.H. Ni, Determining rayleigh damping parameters of soils for finite element analysis, Int. J. Numer. Anal. Meth. Geomech. 31 (2007) 1239–1255.
[43] G. Bazi, J. Gagnon, P. Sebaaly, P. Ullidtz, Effects of rayleigh damping on the subgrade's apparent nonlinearity, J. Transp. Eng. Part B: Pave. 146 (2020) 04020042.
[44] C. Ling, E. David, R. Siddharthan, Comparison of dynamic and static backcalculation moduli for three-layer pavements, Transp. Res. Rec. 1293 (1991) 86–92.
[45] X. Tang, S.M. Stoffels, A.M. Palomino, Evaluation of pavement layer moduli using instrumentation measurements, Int. J. Pavement Res. Technol. 6 (2013).
[46] Q. Xu, J.A. Prozzi, A time-domain finite element method for dynamic viscoelastic solution of layered-half-space responses under loading pulses, Comput. Struct. 160 (2015) 20–39.
[47] X. Zeng. Rubber-modified asphalt concrete for high-speed railway roadbeds. Department of Civil Engineering, Case Western Reserve University: 2005.
[48] M.S. Mamlouk, Use of dynamic analysis 1n predicting field multilayer pavement moduli, Transp. Res. Rec. 1043 (1985) 113.
[49] B. Wang, J. Yang, Analysis of the dynamic responses of crcp and crcp+ ac under the vehicle loading by fem, Pave. Mater. Model. Test. Perform. (2009) 131–139.
[50] V. Valaskova, J. Vlcek, M. Drusa. In Experimental and computational dynamic analysis of the foam concrete as a sub-base layer of the pavement structure, MATEC Web of Conferences, 2018; EDP Sciences: p 13002.
[51] I. Idriss, J. Lysmer, R. Hwang, H. Seed. Quad-4: A computer program for evaluating the seismic response of soil structures by variable damping finite element procedures. Report no. Eerc 73-16. Earthquake Engineering Research Center, University of California, Berkeley 1973.
[52] L. Sun, Y. Duan, Dynamic response of top-down cracked asphalt concrete pavement under a half-sinusoidal impact load, Acta Mech. 224 (2013) 1865–1877.
[53] M. Hudson, I. Idriss, M. Beikae, User's Manual for quad4m: A Computer Program to Evaluate the Seismic Response of Soil Structures Using Finite Element Procedures and Incorporating a Compliant Base, University of California, Davis, US, 1994.
[54] F. Liang, H. Chen, M. Huang, Accuracy of three-dimensional seismic ground response analysis in time domain using nonlinear numerical simulations, Earthq. Eng. Eng. Vib. 16 (2017) 487–498.
[55] A.O. Kwok, J.P. Stewart, Y.M. Hashash, N. Matasovic, R. Pyke, Z. Wang, Z. Yang, Use of exact solutions of wave propagation problems to guide implementation of nonlinear seismic ground response analysis procedures, J. Geotech. Geoenviron. Eng. 133 (2007) 1385–1398.
[56] R. Dobry, I. Oweis, A. Urzua, Simplified procedures for estimating the fundamental period of a soil profile, Bull. Seismol. Soc. Am. 66 (1976) 1293–1321.
[57] Systèmes, D. Abaqus anaslysis user's guide. Solid (Continuum) Elements 2014, 6, 2019.
[58] Z. Song, C. Su, Computation of rayleigh damping coefficients for the seismic analysis of a hydro-powerhouse, Shock Vib. 2017 (2017).
[59] X. Zhong, X. Zeng, J. Rose, Shear modulus and damping ratio of rubber-modified asphalt mixes and unsaturated subgrade soils, J. Mater. Civ. Eng. 14 (2002) 496–502.
[60] X. Zeng, J. Rose, J. Rice, Stiffness and damping ratio of rubber-modified asphalt mixes: Potential vibration attenuation for high-speed railway trackbeds, J. Vib. Control 7 (2001) 527–538.
[61] J. Huang, P. Leandri, G. Cuciniello, M. Losa, Mix design and laboratory characterisation of rubberised mixture used as damping layer in pavements, J. Pavement Eng. (2021) 1–15.